Northeast Indian stalagmite records Pacific decadal climate change: Implications for moisture transport and drought in India

Christopher G. Myers[1], Jessica L. Oster[1], Warren D. Sharp[2], Ralf Bennartz[1], Neil P. Kelley[3], Aaron K. Covey[1], and Sebastian F.M. Breitenbach[4]

[1]Department of Earth and Environmental Sciences, Vanderbilt University, Nashville, Tennessee, USA, [2]Berkeley Geochronology Center, Berkeley, California, USA, [3]National Museum of Natural History, Smithsonian Institute, Washington, District of Columbia, USA, [4]Department of Earth Sciences, University of Cambridge, Cambridge, UK

Abstract Two types of El Niño events are distinguished by sea surface temperature (SST) anomalies centered in the central or eastern equatorial Pacific. The Central Pacific El Niño events (CP-El Niño) are more highly correlated with weakening of the central Indian Summer Monsoon and linked to decadal Pacific climate variability. We present a 50 year, subannually resolved speleothem δ^{18}O record from northeast India that exhibits a significant correlation with northern Pacific decadal variability and central equatorial Pacific SSTs. Accordingly, we suggest that δ^{18}O time series in similar northeast Indian speleothems are effective tools for investigating preinstrumental changes in Pacific climate, including changes in El Niño dynamics. In contrast to central India, rainfall amounts in northeast India are relatively unaffected by El Niño. However, back trajectory analysis indicates that during CP-El Niño events moisture transport distance to northeast India is reduced, suggesting that variations in moisture transport primarily control δ^{18}O in the region.

1. Introduction

The Indian Summer Monsoon (ISM) plays an essential role in structuring the agriculture and economy of India [*Kumar et al.*, 2006; *Douglas et al.*, 2009; *Niranjan Kumar et al.*, 2013]. The ability to predict changes in ISM strength is important for anticipating water shortages [*Kumar et al.*, 2006], yet the complexity of interrelated forcings on ISM variability make accurate monsoon prediction challenging. Reduced monsoon rainfall is strongly correlated with positive anomalies in the El Niño–Southern Oscillation (ENSO) [*Kumar et al.*, 1999, 2006; *Ashok et al.*, 2001; *Shukla et al.*, 2011]. However, not all El Niño events coincide with Indian drought, and this has stymied monsoon prediction efforts [*Kumar et al.*, 2006]. Historical records suggest that droughts associated with reductions in monsoon rainfall are more closely linked to sea surface temperature (SST) anomalies in the central rather than the eastern equatorial Pacific and the occurrence of Central Pacific (CP-) El Niño events [*Kumar et al.*, 2006; *Ashok and Yamagata*, 2009]. CP-El Niño conditions are more effective than Eastern Pacific (EP-) El Niño conditions at forcing drought in central India by shifting the descending arm of the Walker circulation over the eastern equatorial Indian ocean, driving anomalous regional Hadley circulation that suppresses monsoon rainfall [*Krishnamurthy and Goswami*, 2000, *Kumar et al.*, 2006]. Low-frequency, decadal variations in northern Pacific SSTs, such as the Pacific Decadal Oscillation (PDO) and the North Pacific Gyre Oscillation (NPGO) may also influence ISM rainfall through feedbacks with the tropical Pacific and can enhance or suppress the ENSO-ISM relationship. For example, ENSO-related periodicities in ISM rainfall appear to be stronger during PDO-negative phases, whereas droughts associated with El Niño events are more severe during PDO-positive phases [*Sen Roy*, 2011; *Krishnamurthy and Krishnamurthy*, 2014].

CP-El Niños have been growing in strength and frequency since the 1990s [*Lee and McPhaden*, 2010]. It has been suggested that this increase may reflect increased atmospheric greenhouse gases [*Yeh et al.*, 2009]. However, changes in thermocline structure and trade wind strength do not support greenhouse gas forcing as a primary cause of this intensification [*McPhaden et al.*, 2011]. Rather, evidence suggests that the shift may stem from links between ENSO and Pacific decadal variability [*Di Lorenzo et al.*, 2010; *McPhaden et al.*, 2011]. Model simulations indicate increased occurrence of CP- over traditional EP-El Niño events during the mid-Holocene (6 ka) [*An and Choi*, 2014], suggesting past shifts in El Niño flavor could provide insight into present El Niño behavior. Speleothems provide important records of Holocene ISM changes [*Sinha et al.*, 2011; *Berkelhammer et al.*, 2012]

and thus have potential for recording past changes in El Niño behavior. Here we use subannually resolved (7–8 samples per year) speleothem oxygen isotope ($\delta^{18}O_{spel}$) variations over the past 50 years to demonstrate the prospects of stalagmites as archives of variations in Pacific climate, including El Niño dynamics, and highlight the effectiveness of Pacific climate variability to modify ISM precipitation in central and northeast (NE) India.

2. Methods

Stalagmite MAW-0201 was collected in February 2013 from an active drip site in Mawmluh Cave (25°15′44″N, 91°52′54″E, 1160 m above sea level (asl)) in NE India (supporting information Figure S1). The 22 mm aragonite stalagmite was deposited on the exposed surface of a toppled stalagmite (supporting information Figure S2a). MAW-0201 displays laminae consisting of, on average 0.38 mm thick, light-dark couplets (supporting information Figure S2b). Layer counting was performed using ImageJ [*Rasband*, 2004]. Six ~15 mg samples each incorporating ~2 growth layers were drilled for U-Th dating (supporting information Figure S2b).

U-Th analyses were performed at the Berkeley Geochronology Center using a Thermo NEPTUNE *Plus* multicollector, inductively coupled plasma mass spectrometer. Ages, analytical data, and analytical details are provided in the supporting information. Uncertainties of ages are given at the 2σ level and include measurement errors and uncertainties associated with detritus corrections.

Subsamples ($n = 393$) for oxygen isotope analysis were collected at 50 μm spatial resolution, yielding 7–8 samples per lamina. Analyses were carried out at ETH Zürich following *Breitenbach and Bernasconi* [2011]. An in-house carbonate standard (MS2) was used to normalize the data against the Vienne Pee Dee Belemnite (VPDB).

Two age models were constructed using the COPRA package in MATLAB [*Breitenbach et al.*, 2012] (supporting information Figure S3). The first uses six U series dates and 1000 Monte Carlo simulations with polynomial interpolation (pchip) to determine the median age values and 2.5% and 97.5% quantiles, corresponding to ~2σ confidence limits. The second includes layer counts. Both age models agree very well, although in the lower segment the layer counting chronology is ~1–2 years older than the U series-only chronology (supporting information Figure S3). We interpret the U series chronology to be more reliable, as multiple laminae may be deposited in a single year [*Shen et al.*, 2013]. The $\delta^{18}O_{spel}$ time series on the U series-only age model has a varying time step of 0.07–0.58 years. We used linear interpolation to place the time series on a monthly time step for statistical comparison with other climate indices and wavelet analysis. Raw data sets were smoothed for visual comparison using the LOESS smoothing function with a second order locally weighted polynomial set to a span of 0.2 in R [*R Core Team*, 2014].

Continuous wavelet (CWT) and cross-wavelet (XWT) transforms were used to explore changes in the frequency of variability in the MAW-0201 $\delta^{18}O_{spel}$ record through time and investigate linkages between $\delta^{18}O_{spel}$ and local and regional climate. We compared our record to monthly rainfall anomalies recorded at the Cherrapunji meteorological station 2.8 km northeast of Mawmluh Cave (25°30′N, 91°70′E, 1312 m asl) (http://climexp.knmi.nl), and several indices that capture interannual variability in Pacific Ocean climate including SST anomalies in the Niño3 and Niño4 regions of the tropical Pacific, the Pacific Decadal Oscillation (PDO), and the North Pacific Gyre Oscillation (NPGO). All wavelet analyses used the Morlet wavelet and were performed using a MATLAB package provided by the National Oceanography Centre of the Natural Environment Research Council [*Grinsted et al.*, 2004]. All indices used in our wavelet analysis were sufficiently close to a Gaussian distribution to not warrant further transformation. Indices were padded with the average data set value on both sides of the series to reduce edge effects and uncertainties associated with the cone of influence [*Grinsted et al.*, 2004]. Lastly, we computed Pearson's product-moment correlation coefficients (r values) between the $\delta^{18}O_{spel}$ record and coincident SST anomalies across the northern and equatorial Pacific recorded in the Kaplan SST anomaly data set [http://www.esrl.noaa.gov/psd/].

Air mass origin was calculated using the Hybrid Single-Particle Lagrangian Integrated Trajectory model (HYSPLIT4) [*Draxler et al.*, 1999] provided by NOAA's Air Resource Laboratory. Back trajectories were calculated using National Center for Environmental Prediction reanalysis meteorological fields. Back trajectories were calculated daily for the entire study period and a target region 25.25°–25.35°N and 91.25°–91.95°E.
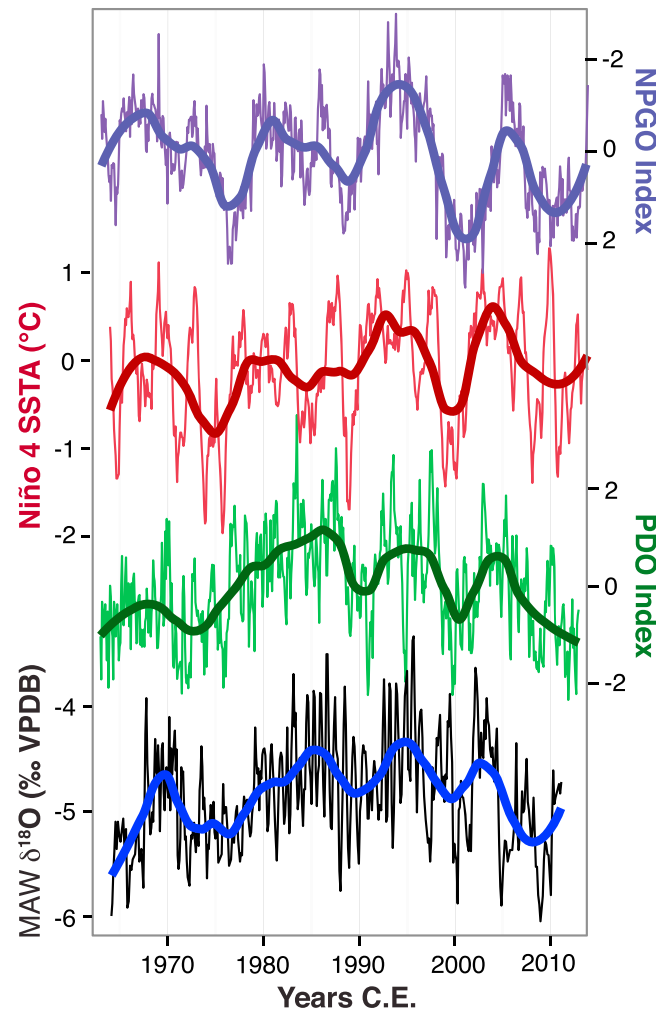
Figure 1. (from bottom to top) $\delta^{18}O_{spel}$, the PDO index (http://jisao. washington.edu/pdo), Niño4 SST anomalies (www.cpc.ncep.noaa.gov), and the NPGO index (y axis reversed) (http://www.o3d.org/npgo/npgo. php). Bold lines are LOESS smoothing (see text).

For each day, 120 back trajectories were started from within this region at heights between 500 and 1500 m above the surface leading to approximately 3600 trajectories each month. Calculations were performed backwards in time for 72 and 96 h (see Supporting Information). Using the back trajectory data set, monthly and seasonal density maps of air mass origin were generated.

3. Results

U-Th analysis of MAW-0201 yields a surface date of 2012.5 ± 2.7 C.E. (Common Era; all errors 2σ; see supporting information Table S1), consistent with active carbonate deposition until collection. The lowermost dated sample, 2 mm from the base, produced a U-Th date of 1966.4 ± 2.1 C.E. The U series-only age model produced in COPRA stretches from 1964 to 2011 (supporting information Figure S3). Layer counting of MAW-0201 revealed 51 distinct layers between the start of aragonite deposition and the top of the sample, with a calculated standard error of 2.1 years (2σ) averaged over three recounts. Comparison of the U-Th ages with the layer counting indicates that the layers are likely annual in nature. We note, however, that the assumption of annual deposition must be treated with care. For example, distinct infiltration periods within a single year might mimic annual laminae [*Shen et al.*, 2013].
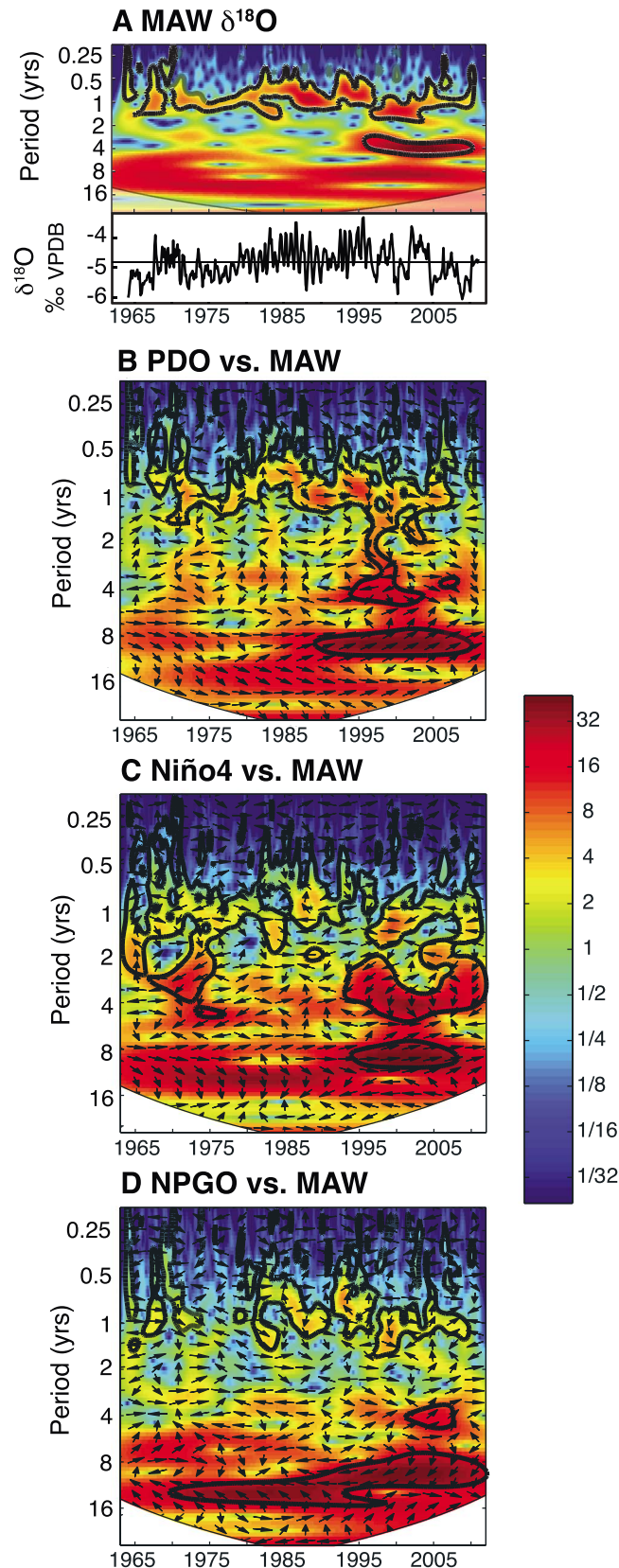
MAW-0201 $\delta^{18}O_{spel}$ ranges from −3.33‰ to −6.05‰ (average −4.84‰) with an external standard deviation of 0.06‰ (Figure 1 and supporting information Figure S4). Visually, MAW-0201 $\delta^{18}O_{spel}$ shows distinct similarities to the PDO index and Niño4 SST anomalies (Figure 1). Over the entire record, $\delta^{18}O_{spel}$ displays a moderate but significant positive correlation with the PDO ($r = 0.31$, $p < 0.001$), a weak but significant positive correlation with Niño4 ($r = 0.12$, $p = 0.003$) and a weak but significant negative correlation with the NPGO ($r = −0.10$, $p = 0.01$) (supporting information Table S2). The CWT of the $\delta^{18}O_{spel}$ time series reveals an annual periodicity that persists throughout the record (Figure 2a). Both, the $\delta^{18}O_{spel}$ time series and CWT indicate a strengthening of the annual periodicity in the late 1970s until the mid-1990s (Figure 2a). A significant ~4 year periodicity appears in the early 1990s. Longer period cyclicity in the $\delta^{18}O_{spel}$ record, varying from 6 to 12 years, is suggested in the CWT but is not identified as significant at the 95% confidence level.

Cross wavelets between $\delta^{18}O_{spel}$ and the PDO and Niño4 indices reveal common, in-phase 8–12 year periodicities, which become significant after 1990 (Figures 2b and 2c). The XWT between $\delta^{18}O_{spel}$ and the Niño3 index is similar to that between $\delta^{18}O_{spel}$ and Niño4 but lacks the strong 8 to 12 year periodicity (supporting information Figure S5). A strong out-of-phase 10–12 year common periodicity is evident between $\delta^{18}O_{spel}$ and the NPGO that switches in the mid-1990s to an 8–10 year periodicity.

A MAW δ^{18}O

B PDO vs. MAW

C Niño4 vs. MAW

D NPGO vs. MAW

4. Discussion

Variations in MAW-0201 aragonite $\delta^{18}O_{spel}$ should primarily reflect changes in the δ^{18}O signature of rainwater ($\delta^{18}O_{precipitation}$) infiltrating into Mawmluh Cave with minimal temporal lag. A 3 year monitoring study of Mawmluh Cave indicates that seepage water transfers the $\delta^{18}O_{precipitation}$ signature into the cave with a lag of less than 1 month, preserving the seasonal signal of ISM rainfall (*Breitenbach et al.* [2015] and supporting information Figure S6). Using the aragonite-water fractionation equation of *Kim et al.* [2007], cave air temperature recorded at the sampling site between January 2010 and March of 2013 (19.4 ± 1.8°C) [*Breitenbach et al.*, 2015], and the most recent $\delta^{18}O_{spel}$ maximum and minimum (−5.97‰ to −4.61‰), we estimate drip water δ^{18}O values of −5.56‰ to −5.16‰ VSMOW. These values fall within the range of measured drip water δ^{18}O collected between 2011 and 2012 (−7.25 to −5.0‰ VSMOW), suggesting that MAW-0201 precipitated close to isotopic equilibrium with drip water.

The $\delta^{18}O_{precipitation}$ in Meghalaya shows no significant correlation with rainfall amount but varies with the source and transport pathway of moisture reaching the region [*Breitenbach et al.*, 2010]. The ISM moisture source is known to vary seasonally from northwestern continental India into the open Indian Ocean and Arabian Sea with the ISM onset, and later into the northern Bay of Bengal (BoB) at the end of the ISM season [*Zhou and Yu*, 2005; *Breitenbach*

Figure 2. (a) CWT and time series of $\delta^{18}O_{spel}$. (b) XWTs between $\delta^{18}O_{spel}$ and the PDO index, (c) Niño4 SST anomalies, and (d) the NPGO index, respectively. Black contoured areas are significant above the 95% confidence level. For B-D, these represent a significant shared periodicity between time series. Right facing arrows represent an in-phase relationship between the two time series, left facing antiphase, and arrows pointing either up or down represent a lag or lead between the indices of 90° or 270°.
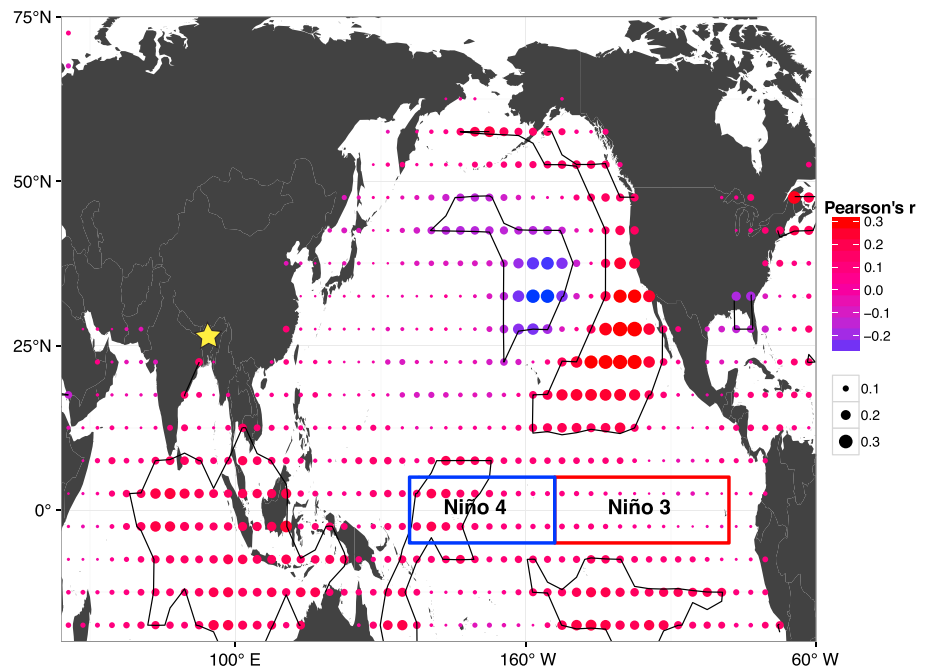
Figure 3. Map of Pearson's product moment correlations (r) between $\delta^{18}O_{spel}$ and SST anomalies for the entire MAW-0201 record (1964–2011) (http://www.esrl.noaa.gov/psd/). Positive correlations are shown in red, negative in blue. Correlation strength denoted by size of the circle and brightness of color. Areas contoured in black are significant above the 99% confidence level. Star shows location of Mawmluh Cave.

et al., 2010]. Rayleigh fractionation on longer transport pathways during the height of the monsoon season leads to ^{18}O depletion of the rainwater, compared to the dry season when pathways are shorter and distillation is limited. Vapor sources are again more localized during the late ISM season, but freshening of BoB surface waters due to ISM runoff leads to source waters and rainfall that are more depleted in ^{18}O [Breitenbach et al., 2010]. The weak correlation between $\delta^{18}O_{spel}$ and monthly precipitation in Cherrapunji during the period corresponding to our record ($r = 0.12$, $p = 0.003$) indicates that the variability in $\delta^{18}O_{spel}$ is largely modulated by ISM moisture transport [Breitenbach et al., 2010], with higher $\delta^{18}O_{spel}$ values indicating shorter transport pathways and/or vapor sources more enriched in ^{18}O as a result of weak ISM circulation.

The PDO and NPGO represent the first and second modes of low-frequency North Pacific SST variability. While the PDO is strongly associated with SST and sea level pressure anomalies in the north and northeast Pacific, the NPGO has a stronger association with anomalies in the northern and tropical central Pacific [Di Lorenzo et al., 2010]. The overall correlation with the PDO, the common in-phase decadal periodicities between $\delta^{18}O_{spel}$ and the PDO and Niño4 SST, as well as the out of phase quasi-decadal common periodicity with the NPGO suggest a significant relationship between decadal variability in the tropical and North Pacific Ocean and $\delta^{18}O_{precipitation}$ in NE India (Figures 1 and 2). This relationship is underscored when $\delta^{18}O_{spel}$ is regressed against the history of SST anomalies across the Pacific for the entire time series (1964–2011). Here significant positive correlations emerge in the northeast Pacific along the western coast of North America extending south of Hawaii, and the central equatorial Pacific, and significant negative correlations emerge in the north central Pacific (Figure 3). This pattern is similar to SST anomalies that develop during PDO-positive phases [Mantua and Hare, 2002] but has stronger correlations with the Niño4 region of the central, rather than the eastern tropical Pacific, similar to the SST anomaly pattern associated with the NPGO [Di Lorenzo et al., 2010].

Comparison of the $\delta^{18}O_{spel}$ and PDO time series (Figure 1) as well as the CWT and XWT suggests that annual frequencies dominate the $\delta^{18}O_{spel}$ record and display larger amplitudes during years characterized by a positive PDO index. This is especially evident in the late 1970s, following the regime shift of 1976–1977 until the late 1990s when PDO shifted into a negative phase [Mantua and Hare, 2002]. In contrast, during PDO-negative phases, $\delta^{18}O_{spel}$ shows evidence of stronger multiannual periodicity (Figure 2a) in part shared with Niño4 SST (Figure 2c). The complicated phasing patterns between $\delta^{18}O_{spel}$ and Niño4 SST may reflect

a seasonal lag between the development of tropical Pacific SST anomalies and their impact on the ISM (supporting information Figure S7), but it is not possible to evaluate such lags with certainty given precision of the MAW-0201 chronology. However, these observations are consistent with comparisons of monsoon rainfall across India and the PDO that suggest weakening of ENSO-related periodicities during PDO-positive phases [*Sen Roy*, 2011]. Although a positive PDO has been linked to drought conditions on the Indian subcontinent, we observe only a weakly significant correlation between monsoon rainfall amount in Cherrapunji and PDO index over the interval covered by the $\delta^{18}O_{spel}$ record ($r = 0.09$, $p = 0.032$).

The strong, in-phase common periodicity and correlation between the $\delta^{18}O_{spel}$ record and SSTs in the Niño4 region (Figures 2c and 3) also suggest a strengthening tie between the central tropical Pacific and the ISM since the 1990s. Positive SST anomalies in the Niño4 region are closely associated with CP-El Niño events [*Lee and McPhaden*, 2010; *Yu et al.*, 2012], which are known to display strong decadal variability [*Weng et al.*, 2007]. Although CP-El Niño events are associated with drought in central India [*Kumar et al.*, 2006], NE India typically experiences normal rainfall during CP-El Niño years [*Gadgil et al.*, 2002, 2005]. Comparison of monthly rainfall in Cherrapunji with the Oceanic Niño Index that is based on SST anomalies in the Niño3.4 region (overlapping portions of both Niño3 and 4) indicates there is no consistent relationship between NE India rainfall and ENSO state over the period of our record (supporting information Figure S8).

The lack of correlation between SST anomalies in the equatorial Pacific and Cherrapunji rainfall amounts further suggests that the in-phase relationship observed between $\delta^{18}O_{spel}$ and Niño4 SST reflects changes in ISM moisture transport rather than rainfall amount. Accordingly, shorter moisture transport pathways and/or moisture sources enriched in ^{18}O are associated with positive SST anomalies in the Niño4 region. The stronger relationship between $\delta^{18}O_{spel}$ and Niño4 SST over Niño3 also suggests that CP-El Niño events influence moisture transport to NE India more effectively than EP-El Niño events. To corroborate these hypotheses, we performed 72 and 96 h back trajectory analyses for the months covering the ISM season (May through September) for years characterized by CP- and EP-El Niño events and La Niña and ENSO neutral years (Figure 4). We chose years in which Pacific SST anomalies occurred during the monsoon season. The reanalysis data available for the HYSPLIT simulations limits us to events occurring between 1982 and the present. The results of this analysis indicate that, during CP-El Niño years, trajectories are more likely to originate further north in the BoB at the height of the monsoon season, whereas during EP-El Niño years the moisture trajectories originate further southwest in the southern BoB and open Indian Ocean (Figure 4). Both kinds of El Niño result in shorter trajectories in June than during La Niña and ENSO neutral years. In June of CP-El Niño years, 52% of ISM trajectories originate north of 15°N compared to 42% during EP-El Niño years, 34% during La Niña years, and 30% during neutral years (Figure 4). By the end of the ISM season in September, the majority of trajectories originate north of 15°N for all ENSO states (supporting information Figure S9). These results suggest that moisture trajectories to NE India at the height of the monsoon season are sensitive to the spatial configuration of SST anomalies in the equatorial Pacific, with central Pacific anomalies leading to shorter transport paths, possibly related to enhanced subsidence over central India [*Kumar et al.*, 2006].

Di Lorenzo et al. [2010] outline a mechanism by which SST anomalies associated with CP-El Niño events force changes in atmospheric circulation across the North Pacific that are then expressed through the NPGO [*Di Lorenzo et al.*, 2008]. This dynamical link is similar to that proposed for the traditional EP-El Niño and the PDO via an atmospheric bridge through the Aleutian Low [*Alexander et al.*, 2002; *Di Lorenzo et al.*, 2010]. The $\delta^{18}O_{spel}$ record and the NPGO share a strong common antiphased periodicity that shifts from 10–12 years to 8–10 years in the 1990s at the same time that the in-phase 8–10 year periodicities strengthen between $\delta^{18}O_{spel}$, the PDO, and Niño4. Although the overall correlation with the $\delta^{18}O_{spel}$ record is stronger for the PDO ($r = 0.31$, $p < 0.001$) than the NPGO ($r = -0.10$, $p = 0.01$), the pattern of correlations between the $\delta^{18}O_{spel}$ record and SST anomalies in the Pacific documents significant ties with the central equatorial Pacific and the North Pacific, with patterns reminiscent of both the PDO and the NPGO. Possibly, changes in Pacific SST gradients associated with the PDO and/or NPGO act to amplify or suppress the effects of tropical SST anomalies associated with El Niño events [*Sen Roy*, 2011] leading to interdecadal differences in the degree of Walker and Hadley circulation modification that influence moisture transport to NE India. Furthermore, observed changes in $\delta^{18}O_{spel}$ since the 1990s suggest a strengthening of the relationship between the tropical and North Pacific and moisture transport to India, coincident with a shift in ENSO dynamics [*Yeh et al.*, 2009], that might have consequences for ISM precipitation in the near future.
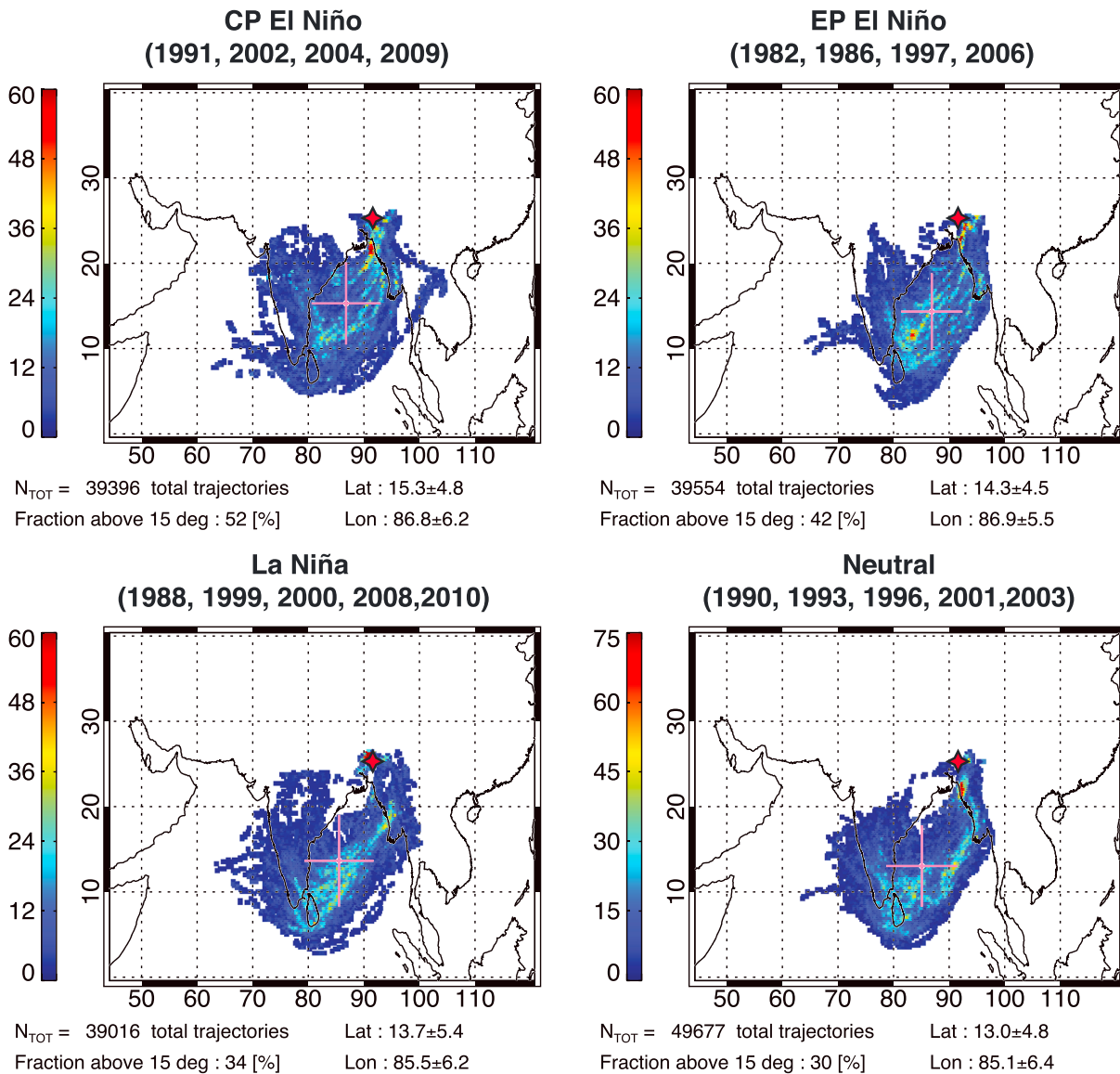
Figure 4. HYSPLIT back trajectory analyses for June of CP- and EP-El Niño, La Niña, and ENSO neutral periods. Back trajectories were calculated at varying heights over a 72 h interval originating from a rectangular region over Meghalaya (approximately 75 × 11 km, red diamond). Shading represents number of trajectories originating per 0.25 × 0.25° per month. Crosses and coordinates give mean latitude and longitude of all trajectories with (2σ) standard deviations (for results of 96 h trajectories see supporting information Figure S10).

The high-resolution $\delta^{18}O_{spel}$ record that we have developed for the past 50 years demonstrates that speleothems from NE India are sensitive to SST anomalies in the northern and central equatorial Pacific. Thus, they provide insights into decadal variability in the Pacific as well as ENSO-ISM teleconnections. Although CP-El Niño events do not alter the amount of precipitation over NE India significantly, they do diminish monsoon precipitation in central India and lead to shorter moisture trajectories reaching the NE. Likewise, changes in the PDO act to amplify the annual variability and modulate the influence of ENSO on the ISM throughout India. Our record reinforces recent observations that the $\delta^{18}O_{precipitation}$, and therefore the $\delta^{18}O$ of speleothems, in South and East Asia may not reflect precipitation amount but rather moisture transport and source [*Breitenbach et al.*, 2010; *Pausata et al.*, 2011]. This further suggests that additional proxies that are more sensitive to changes in moisture availability must be assessed before evaluating past changes in aridity based on speleothem records.

5. Conclusions

Stalagmite MAW-0201 grew rapidly over the past 50 years and permits comparison of $\delta^{18}O_{spel}$ with instrumental data at unprecedented temporal resolution. Our record demonstrates that the isotopic signature of rainfall over NE India is sensitive to conditions in the northern and central equatorial Pacific and supports observations that CP-El Niño events are more effective at modifying ISM precipitation than EP-El Niño events [*Kumar et al.*, 2006; *Weng et al.*, 2007]. CP-El Niños lead to drought in central India (but not necessarily in NE India) and trigger a shift to more localized storm trajectories reaching NE India. Our record further suggests that the ENSO-ISM relationship is modulated by the PDO [*Sen Roy*, 2011] and thus has implications for understanding teleconnections between Pacific climate and the ISM under different boundary conditions. Comparison between paleoclimate model simulations and fast growing stalagmites similar to MAW-0201 could assess the degree of stationarity in the relationship between North Pacific Decadal Variability and the ENSO-ISM relationship under different boundary conditions and evaluate the relative impact of CP- and EP-El Niño events through the Holocene when such changes have been suggested [*An and Choi*, 2014]. Detailed understanding of how decadal variability in the Pacific has disrupted ISM precipitation in the past further serves to improve our comprehension of how the ISM is likely to evolve under future climate conditions.

References

Alexander, M., I. Bladé, M. Newman, J. R. Lanzante, N.-C. Lau, and J. D. Scott (2002), The atmospheric bridge: The influence of ENSO teleconnections on air-sea interaction over the global oceans, *J. Clim.*, *15*(16), 5163–5174, doi:10.1175/1520-0442(2002)015<2205:TABTIO>2.0.CO;2.

An, S.-I., and J. Choi (2014), Mid-Holocene tropical Pacific climate state, annual cycle, and ENSO in PMIP2 and PMIP3, *Clim. Dyn.*, *43*(3–4), 957–970, doi:10.1007/s00382-013-1880-z.

Ashok, K., and T. Yamagata (2009), Climate change: The El Niño with a difference, *Nature*, *461*(7263), 481–484, doi:10.1038/461481a.

Ashok, K., Z. Guan, and T. Yamagata (2001), Impact of the Indian Ocean dipole on the relationship between the Indian monsoon rainfall and ENSO, *Geophys. Res. Lett.*, *28*(23), 4499–4502, doi:10.1029/2001GL013294.

Berkelhammer, M., A. Sinha, L. Stott, H. Cheng, F. S. R. Pausata, and K. Yoshimura (2012), An abrupt shift in the Indian Monsoon 4000 years ago, in *Climates, Landscapes, and Civilizations*, Geophys. Monogr. Ser., edited by L. Giosan et al., AGU, Washington, D. C., doi:10.1029/2012GM001207.

Breitenbach, S. F., and S. M. Bernasconi (2011), Carbon and oxygen isotope analysis of small carbonate samples (20 to 100 g) with a GasBench II preparation device, *Rapid Commun. Mass Spectrom.*, *25*(13), 1910–1914, doi:10.1002/rcm.5052.

Breitenbach, S. F., J. F. Adkins, H. Meyer, N. Marwan, K. K. Kumar, and G. H. Haug (2010), Strong influence of water vapor source dynamics on stable isotopes in precipitation observed in Southern Meghalaya, NE India, *Earth Planet. Sci. Lett.*, *292*(1), 212–220, doi:10.1016/j.epsl.2010.01.038.

Breitenbach, S. F. M., et al. (2012), COnstructing Proxy Records from Age models (COPRA), *Clim. Past*, *8*(5), 1765–1779, doi:10.5194/cp-8-1765-2012.

Breitenbach, S. F. M., F. A. Lechleitner, H. Meyer, G. Diengdoh, D. Mattey, and N. Marwan (2015), Cave ventilation and rainfall signals in dripwater in a monsoonal setting—A monitoring study from NE India, *Chem. Geol.*, *402*, 111–124, doi:10.1016/j.chemgeo.2015.03.011.

Di Lorenzo, E., et al. (2008), North Pacific Gyre Oscillation links ocean climate and ecosystem change, *Geophys. Res. Lett.*, *35*, L08607, doi:10.1029/2007GL032838.

DiLorenzo, E., et al. (2010), Central Pacific El Niño and decadal climate change in the North Pacific Ocean, *Nat. Geosci.*, *3*, 762–765, doi:10.1038/ngeo984.

Douglas, E., A. Beltrán-Przekurat, D. Niyogi, R. A. Pioelke Sr., and C. J. Vörösmarty (2009), The impact of agricultural intensification and irrigation on land-atmosphere interactions and Indian monsoon precipitation—A mesoscale modeling perspective, *Global Planet. Change*, *67*(1), 117–128, doi:10.1016/j.gloplacha.2008.12.007.

Draxler, R. R., B. Stunder, G. Rolph, A. Stein, and A. Taylor (1999), HYSPLIT4 user's guide, NOAA Technical Memorandum ERL ARL, 230, 35.

Gadgil, S., J. N. Srinivasan, S. Ravi, K. K. Kumar, A. A. Munot, and R. K. Kumar (2002), On forecasting the Indian summer monsoon: The intriguing season of 2002, *Curr. Sci.*, *83*(4), 394–403.

Gadgil, S., M. Rajeevan, and R. Nanjundiah (2005), Monsoon prediction—Why yet another failure?, *Curr. Sci.*, *88*(9), 1389–1400.

Grinsted, A., J. C. Moore, and S. Jevrejeva (2004), Application of the cross wavelet transform and wavelet coherence to geophysical time series, *Nonlinear Process. Geophys.*, *11*(5/6), 561–566, doi:10.5194/npg-11-561-2004.

Kim, S.-T., J. R. O'Neil, C. Hillaire-Marcel, and A. Mucci (2007), Oxygen isotope fractionation between synthetic aragonite and water: Influence of temperature and Mg^{2+} concentration, *Geochim. Cosmochim. Acta*, *71*, 4704–4715, doi:10.1016/j.gca.2007.04.019.

Krishnamurthy, L., and V. Krishnamurthy (2014), Influence of PDO on South Asian summer monsoon and monsoon-ENSO relation, *Clim. Dyn.*, *42*(9–10), 2397–2410, doi:10.1007/s00382-013-1856-z.

Krishnamurthy, V., and B. N. Goswami (2000), Indian monsoon-ENSO relationship on interdecadal timescale, *J. Clim.*, *13*(3), 579–595, doi:10.1175/1520-0442(2000)013<0579:IMEROI>2.0.CO;2.

Kumar, K. K., B. Rajafopalan, and M. A. Cane (1999), On the weakening relationship between the Indian Monsoon and ENSO, *Science*, *284*(5423), 2156–2159, doi:10.1126/science.284.5423.2156.

Kumar, K. K., B. Rajafopalan, M. Hoerling, G. Bates, and M. A. Cane (2006), Unraveling the mystery of Indian Monsoon failure during El Niño, *Science*, *314*(5796), 115–119, doi:10.1126/science.1131152.

Lee, T., and M. J. McPhaden (2010), Increasing intensity of El Niño in the central-equatorial Pacific, *Geophys. Res. Lett.*, *37*, L14603, doi:10.1029/2010GL044007.

Mantua, N. J., and S. R. Hare (2002), The Pacific Decadal Oscillation, *J. Oceanogr.*, *58*, 35–44, doi:10.1023/A:1015820616384.

McPhaden, M. J., T. Lee, and D. McClurg (2011), El Nino and its relationship to changing background conditions in the tropical Pacific Ocean, *Geophys. Res. Lett.*, *38*, L15709, doi:10.1029/2011GL048275.

Niranjan Kumar, K., M. Rajeevan, D. S. Pai, A. K. Srivastava, and B. Preethi (2013), On the observed variability of monsoon droughts over India, *Weather Clim. Extremes*, *1*, 42–50, doi:10.1016/j.wace.2013.07.006.

Pausata, F. S. R., D. S. Battisti, K. H. Nisangcioglu, and C. M. Bitz (2011), Chinese stalagmite δ^{18}O controlled by changes in the Indian monsoon during a simulated Heinrich event, *Nat. Geosci.*, *4*(7), 474–480, doi:10.1038/ngeo1169.

R Core Team (2014), R: A language and environment for statistical computing, R Foundation for Statistical Computing, Vienna, Austria. [Available at http://www.R-project.org/.]

Rasband, W. S. (2004), *ImageJ*, National Institutes of Health, Bethesda, Maryland. [Available at http://rsb.info.nih.gov/ij/.]

Sen Roy, S. (2011), Identification of periodicity in the relationship between PDO, El Niño and peak monsoon rainfall in India using S-transform analysis, *Int. J. Climatol.*, *31*, 1507–1517, doi:10.1002/joc.2172.

Shen, C.-C., K. Lin, W. Duan, X. Jiang, J. W. Partin, R. L. Edwards, H. Cheng, and M. Tan (2013), Testing the annual nature of speleothem banding, *Sci. Rep.*, *3*, doi:10.1038/srep02633.

Shukla, R. P., K. C. Tripati, A. C. Pandey, and I. M. L. Das (2011), Prediction of Indian summer monsoon rainfall using Niño indices: A neural network approach, *Atmos. Res.*, *102*(1), 99–109, doi:10.1016/j.atmosres.2011.06.013.

Sinha, A., M. Berkelhammer, L. Stott, M. Mudelsee, H. Cheng, and J. Biswas (2011), The leading mode of Indian Summer Monsoon precipitation variability during the last millennium, *Geophys. Res. Lett.*, *38*, L15703, doi:10.1029/2011GL047713.

Weng, H., K. Ashok, S. K. Behera, S. A. Rao, and T. Yamagata (2007), Impacts of recent El Niño Modoki on dry/wet conditions in the Pacific rim during boreal summer, *Clim. Dyn.*, *29*(2–3), 113–129, doi:10.1007/s00382-007-0234-0.

Yeh, S.-W., J.-S. Kug, B. Dewitte, M.-H. Kwon, B. P. Kirtman, and F.-F. Jin (2009), El Niño in a changing climate, *Nature*, *461*(7263), 511–514, doi:10.1038/nature08316.

Yu, J.-Y., Y. Zou, S. T. Kim, and T. Lee (2012), The changing impact of El Niño on US winter temperatures, *Geophys. Res. Lett.*, *39*, L15702, doi:10.1029/2012GL052483.

Zhou, T.-J., and R.-C. Yu (2005), Atmospheric water vapor transport associated with typical anomalous summer rainfall patterns in China, *J. Geophys. Res.*, *110*, D08104, doi:10.1029/2004JD005413.